Draft version March 14, 2013
Preprint typeset using LaTeX style emulateapj v. 12/16/11

MULTI-WAVELENGTH RADIO CONTINUUM EMISSION STUDIES OF DUST-FREE RED GIANTS

Eamon O'Gorman[1], Graham M. Harper[1], Alexander Brown[2], Stephen Drake[3], and Anita M.S. Richards[4]

Draft version March 14, 2013

ABSTRACT

Multi-wavelength centimeter continuum observations of non-dusty red giants directly sample their wind acceleration zones where most of the energy that drives their mass loss is being deposited. These stars are feeble thermal emitters at these wavelengths however, and previous observations have provided only a small number of modest signal-to-noise measurements accumulated over many years. Here, we present multi-wavelength Karl G. Jansky Very Large Array (VLA) thermal continuum observations of the acceleration zones of two dust-free red giants, Arcturus (α Boo: K2 III) and Aldebaran (α Tau: K5 III). Uniquely, these multi-wavelength observations were mostly carried out within a few days of each other so any long term variability that may exist can be ignored. We report the first detections at many wavelengths for each star including a detection at 10 cm (3.0 GHz; S-band) for both stars and a 20 cm (1.5 GHz; L-band) detection for α Boo. This is the first time single (non-binary) luminosity class III red giants have been observed at such long continuum wavelengths. These long wavelength flux density measurements sample the outer layers of the stars atmosphere where the wind velocity is approaching (or possibly has reached) its terminal value and the ionization balance is becoming *frozen-in*. As a result, they are important empirical inputs for future atmospheric models. We present spectral energy distributions for both stars and compare these with previous measurements and published semi-empirical models. The marked deviations between our data and existing semi-empirical models highlight the need for new atmospheric models to be developed. The derived spectral indices are discussed in relation to the possible properties of the stellar atmospheres and a simple analytical atmospheric model is developed for α Boo which is in close agreement to the observed flux densities at long wavelengths.

Keywords: circumstellar matter — Stars: individual: (α Boo, α Tau) — Stars: late-type — Stars: chromospheres — Stars: winds, outflows — Radio continuum: stars

1. INTRODUCTION

Mass loss from late-type evolved stars plays a crucial role in both stellar and galactic evolution and ultimately provides part of of the material required for the next generation of stars and planets. Despite the importance of this phenomenon and decades of study, the mechanisms that drive winds from evolved spectral-type K through mid-M stars remain an enduring mystery (clearly laid out by Holzer & MacGregor (1985) but still unsolved, e.g. Crowley et al. 2009). There is insufficient atomic, molecular, or dust opacity to drive a radiation-driven outflow and acoustic/pulsation models cannot drive the observed mass loss rates (Sutmann & Cuntz 1995). Optical and ultraviolet observations reveal an absence of hot wind plasma and the winds are thus too cool to be Parker-type thermally-driven flows (e.g. Linsky & Haisch 1979; Ayres et al. 1981).

Magnetic fields are most likely involved in the mass loss process, although current magnetic models are also unsuccessful. Exquisite high signal-to-noise (S/N) ratio *Hubble* ultraviolet (UV) spectra have revealed that the 1-D linear Alfvén wave-driven wind models of the 1980s (e.g., Hartmann & MacGregor 1980) are untenable. These models predict chromospheres as integral parts of turbulently extended and heated wind acceleration zones, but the theoretical line profiles and electron densities do not agree with the *Hubble* spectra, e.g., Judge & Carpenter (1998). One important property of cool evolved star winds gleaned from UV spectra is that, for the most part, the red giant winds accelerate in a quasi-steady manner and are not the result of ballistic ejecta. A new generation of theoretical models with outflows driven within diverging magnetic flux tubes have now emerged (Falceta-Gonçalves et al. 2006; Suzuki 2007) but these too are not yet in agreement with observations (Crowley et al. 2009). It has also been suggested that the winds may be driven by some form of magnetic pressure acting on very highly clumped wind material (Eaton 2008) but Harper (2010) does not find support for this hypothesis. Progress in this field continues to be driven by observations that provide new insights into the mass loss problem.

1.1. *Radio Continuum Observations*

Although studies of wind-scattered UV and optical line profiles have provided clues to the mass loss rates and radial distribution of the mean and turbulent velocity fields, the thermal structure remains poorly constrained. In the UV, the source function is very sensitive to electron temperature (i.e. $S_\nu \propto e^{-h\nu/kT}$) and so a localized hot plasma component in a dynamic atmosphere can completely dominate the temporally and spatially averaged emission and not reflect the global mean value. At

[1] School of Physics, Trinity College Dublin, Dublin 2, Ireland
[2] Center for Astrophysics and Space Astronomy, University of Colorado, 389 UCB, Boulder, CO 80309, USA
[3] NASA Goddard Space Flight Center, Greenbelt, MD 20771, USA
[4] Jodrell Bank Centre for Astrophysics, School of Physics and Astronomy, University of Manchester, Manchester M13 9PL, UK

radio wavelengths however, the source function is thermal and is just the Rayleigh-Jeans tail of the Planck function, which is linear in electron temperature (i.e. $S_\nu = 2kT\nu^2/c^2$) and so should give a more appropriate estimate of the thermal radial wind structure. It is this value that controls the atomic level populations and ionization that feed into UV spectroscopic analyses. This value is also needed to quantify the implied thermal heating supplied to the wind by the unknown driving source/sources, and thus derive constraints on potential mass loss mechanisms.

In the cm-radio regime the radio opacity strongly increases with wavelength (i.e. $\kappa \propto \lambda^{2.1}$) so the longer wavelengths sample the extended layers of the stars atmosphere thus essentially providing us with spatial information about the star's mass outflow region. The thermodynamic properties in this spatial region control the ionization in the far wind because the ionization balance, which also controls the cooling rates, becomes *frozen-in* at these radii due to advection. Furthermore, it is these outer extended regions of the star's atmosphere that contribute to the commonly seen P Cygni line profiles in the UV. In these profiles the line-of-sight absorption caused by the star's wind is superimposed on the blueshifted emission. Thus, centimeter radio continuum observations can provide a test of models based on these UV profiles. In this paper we directly compare our new Karl G. Jansky Very Large Array (VLA) observations with atmospheric models derived from UV analysis.

1.2. *Sample Selection*

Currently the most detailed spatial information about the atmospheres of K and early M evolved stars is obtained from eclipsing binaries such as the symbiotic and ζ Aurigae systems (e.g. Baade et al. 1996; Eaton 2008; Crowley et al. 2008). Even though these systems offer us the best opportunity to obtain information on the dynamics and thermodynamics at various heights in the evolved star's atmosphere, the very nature of the binary system may introduce further complexities. For example, the orbital separation is often within the wind acceleration region and one could expect wind accretion and flow perturbations to be present (e.g. Chapman 1981). In fact, using the 'old' VLA, Harper et al. (2005) confirm that the velocity structure of of ζ Aurigae is not typical of single stars with similar spectral types.

In order to avoid the assumed additional complexities of a companion, we have selected two single luminosity class III red giants: Arcturus (α Boo: K2 III) and Aldebaren (α Tau: K5 III). These nearby red giants have been extensively studied at other wavelengths and their stellar parameters, which are briefly summarized in Table 1, are accurately known. These stars are predicted to be point sources at all frequencies in all VLA configurations so our radio observations measure their total flux density, F_ν. Moreover both stars have existing semi-empirical 1-D chromospheric and wind models which we directly compare to our data in this paper.

2. OBSERVATIONS AND DATA REDUCTION

Observations of α Boo and α Tau were carried out with the VLA during February 2011 at Q, Ka, K, X, C, and S-band in B-configuration (PI: Harper; program 10C-105). α Boo was also observed at S and L-band in July 2012 when the VLA was again in B-configuration (PI: O'Gorman; program 12A-472). Some details of these observations are given in Table 2. For the 2011 observations, the correlator was set up with two 128 MHz sub-bands centered on the frequencies listed in Table 2. Each sub-band had sixty-four channels of width 2 MHz and four polarization products (RR, LL, RL, LR). For the S and L-band observations in 2012, the 1-2 GHz and 2-4 GHz frequency ranges were both divided into 16 sub-bands, each with sixty-four channels. The channel width was 2 and 1 MHz for S and L-band, respectively.

Table 1
Some properties of our red giant sample.

	α Boo	α Tau
Spectral Type	K2 III	K5 III
Effective Temperature (K)	4294 ± 30	3970 ± 49
Distance (pc)	20.43	11.26
Angular Diameter (mas)	21.0 ± 0.2	20.2 ± 0.3
Mass Loss Rate ($M_\odot$ yr^{-1})	2×10^{-10}	1.6×10^{-11}
Wind Temperature (K)	$\sim 10,000$	$< 10,000$
Wind Terminal Velocity	~ 40 km s^{-1}	~ 30 km s^{-1}
Semi-empirical model	Drake (1985)	McMurry (1999)

Note. — Effective temperatures and photospheric diameters are from di Benedetto (1993). Distances are from van Leeuwen (2007). Mass loss rates are from Drake (1985) and Robinson et al. (1998).

Both α Boo and α Tau were slightly offset from the phase-center by ~ 5 synthesized beam widths in order to avoid possible errors at phase-center. All scheduling blocks (SBs) were kept to ≤ 2.5 hours of duration to improve their likelihood of being scheduled. For the high frequency observations (i.e. Q, Ka, and K-bands) we used the *fast switching* technique which consisted of rapidly alternating observations of the target source and a nearby unresolved phase calibrator. The total cycle times for the Q, Ka, and K-band observations were 160, 230, and 290 s, respectively. For both target sources these high frequency observations were combined into a single 2 hour observing track and commenced with X-band reference pointing with solutions being applied on-line. After X-band pointing the target source was observed at Q-band to insure the best pointing solutions were used. The lower frequencies tracks were composed of repeatedly interleaving observations of the target source and a nearby phase calibrator but had much longer cycle times. The primary calibration sources 3C286 and 3C138 were observed at the end of all tracks and were used to measure the complex bandpass and set the absolute flux for α Boo and α Tau, respectively.

The data were flagged, calibrated, and imaged within the Common Astronomical Software Application (CASA; McMullin et al. 2007) package. Data deemed to be bad by the VLA online system were flagged, as were pure zeros, non-operational antennae, dummy scans at the beginning of each track, and poorly performing antennae. Visual inspection of each scan was carried out to determine if data at the beginning or end of these scans needed to be flagged (a process known as *quacking*). For the 2011 low frequency data the two sub-bands were centered at relatively radio frequency interference (RFI) free regions of the bandpass and only a very small amount of RFI had to be flagged. The 2012 wide-band data was ini-

Table 2
VLA Observations

Star	Date	Band	Frequency[a] (GHz)	Wavelength (cm)	Time on Star (hr)	Bandwidth (GHz)	Number of Antennae[b]	Phase Calibrator
α Boo	2011 Feb 22	Q	43.3	0.7	0.3	0.256	22	J1357+1919
α Boo	2011 Feb 22	Ka	33.6	0.9	0.2	0.256	23	J1357+1919
α Boo	2011 Feb 22	K	22.5	1.3	0.4	0.256	24	J1357+1919
α Boo	2011 Feb 11	X	8.5	3.5	0.3	0.256	18	J1415+1320
α Boo	2011 Feb 11	C	5.0	6.0	0.5	0.256	21	J1415+1320
α Boo	2011 Feb 13	S	3.1	9.5	1.8	0.256	12	J1415+1320
α Boo	2012 Jul 19	S	3.0	10.0	0.7	2.0	23	J1415+1320
α Boo	2012 Jul 20	L	1.5	20.0	1.6	1.0	23	J1415+1320
α Tau	2011 Feb 11	Q	43.3	0.7	0.3	0.256	22	J0431+1731
α Tau	2011 Feb 11	Ka	33.6	0.9	0.2	0.256	19	J0449+1121
α Tau	2011 Feb 11	K	22.5	1.3	0.4	0.256	21	J0449+1121
α Tau	2011 Feb 13	X	8.5	3.5	0.5	0.256	25	J0449+1121
α Tau	2011 Feb 13	C	5.0	6.0	1.2	0.256	21	J0449+1121
α Tau	2011 Feb 12	S	3.1	9.5	1.8	0.256	11	J0431+2037

[a] Central frequency of selected bandpass.
[b] Number of available antennae remaining after flagging.

tially Hanning smoothed (combining adjacent frequency channels with weights 0.25, 0.5, and 0.25) to suppress Gibbs ringing. We manually flagged entire sub-bands that were badly contaminated with RFI. The *testautoflag* task was then used to conservatively flag RFI from all sources and any remaining RFI was manually flagged.

In order to calibrate the data, we solved for the complex gains of the calibration sources while applying the bandpass solution, which was derived from the relevant aforementioned flux calibrators. The amplitude gains of the phase calibrators were scaled according to values derived from the flux calibrators using the "Perley-Butler 2010" flux density standard. At the time, no Ka or S-band flux density standard models were available so instead for these we used the K and L-band models, respectively. The more frequently observed phase calibrators were then used to calibrate the amplitude and phases of the targets. Atmospheric opacity corrections were also applied to the high frequency data sets using the average of a seasonal model (based on many years of measurements) and information from the weather station obtained during the observations.

The visibilities were then both Fourier transformed and deconvolved using the CASA *clean* task in multi-frequency synthesis imaging mode, which separately grids the the multiple spectral channels onto the *u-v* plane and therefore improves the overall *u-v* coverage. We used natural weighting for maximum sensitivity and the cell size was chosen so that the synthesized beam was about five pixels across. For the high frequencies it was usually sufficient to place just one CLEAN circle around the target source. For the low frequencies however, the image sizes were usually set to a few times the size of the primary beam so that nearby strong serendipitous sources could be CLEANed thus reducing their sidelobe contamination of the final image. These images were CLEANed interactively, with w-term correction, down to about the 3σ level with clean boxes placed around sources as they appeared in the residual image. All images were corrected for primary beam attenuation.

Three different methods were used to calculate the flux density from the unresolved target sources in each image:

1. by taking the peak pixel value from the source
2. by manually integrating the flux density around the source
3. by fitting an elliptical Gaussian model to the source and deriving the integrated flux density using the CASA *imfit* task.

Each of these values along with the image root mean square (rms) noise measured from adjacent background regions and fitting error produced by *imfit* are given in Table 3. We assume absolute flux density scale systematic uncertainties of 3% at all frequencies.

3. RESULTS

Apart from α Boo at C-band and α Tau at S-band, detections were made in both sub-bands for the 2011 data. The flux densities of the targets in each sub-bands were found to be the same within their uncertainties so we do not present these values here. Instead we give the values from the radio maps produced by concatenating the two sub-bands. We present in Table 3 the target flux densities extracted from these concatenated radio maps. In the following two sections we briefly discuss the properties of these radio maps for both targets.

3.1. *α Boo Radio Maps*

High S/N detections ($> 19\sigma$) of α Boo were made at 22.5, 33.6, and 43.3 GHz. Some residuals of the dirty beam remained in the CLEANed maps due to the paucity of uv-coverage in these short high frequency observations. The lower frequencies maps were contaminated by the emission of a strong radio source located 186″ northwest of α Boo. This source was reported by Drake & Linsky (1986) and their flux of 25 mJy at 4.9 GHz is in close agreement with our measurement of 23.2 mJy at the same frequency. We find the source to have a spectral index of -1.4 and its flux reaches 80.3 mJy at 1.6 GHz. Surprisingly we do not detect α Boo in the higher frequency sub-band at 5.0 GHz (C-band) so the values given in Table 3 are taken from the lower frequency sub-band only. We obtain good detections ($> 5\sigma$) of the star for both epochs at $\sim$3 GHz (S-band) and the peak flux densities agree within their uncertainties. We can therefore safely assume that the 1.5 GHz (L-band) flux has not changed significantly over that period either, and

Table 3
VLA Fluxe Densities of α Boo and α Tau

	Band	Frequency[a] (GHz)	Peak F_ν (mJy)	Integrated F_ν (mJy)	*Imfit* Integrated F_ν (mJy)	Image rms (Jy beam^{-1})	*Imfit* Fitting Error (mJy)
α Boo (K2 III)	Q	43.28	5.941	6.093	6.420	0.301	0.261
	Ka	33.56	4.159	4.319	4.489	0.083	0.090
	K	22.46	1.827	1.784	1.809	0.043	0.050
	X	8.46	0.510	0.514	0.532	0.030	0.019
	C	4.90	0.214	0.144	0.159	0.035	0.009
	S	3.15	0.148	0.135	0.160	0.028	0.010
	S	2.87	0.127	0.118	0.116	0.012	0.016
	L	1.63	0.067	0.068	0.090	0.013	0.015
α Tau (K5 III)	Q	43.28	3.672	3.734	4.082	0.259	0.183
	Ka	33.56	2.188	1.962	2.125	0.091	0.070
	K	22.46	1.864	1.881	2.069	0.042	0.083
	X	8.46	0.296	0.287	0.281	0.014	0.015
	C	4.96	0.147	0.167	0.176	0.010	0.010
	S	3.15	0.062	0.043	-	0.017	-

[a] Frequency of final image produced using *clean*'s multi-frequency synthesis imaging mode.

so can safely be included in any analysis. The map at L-band was highly contaminated by the emission of the strong source north-west of α Boo but the star is still detected at the 5σ level. There is a slight positional offset of $1''$ between the position of the peak flux density at 1.5 and at 3.0 GHz for the 2012 data, which were taken within 1 day of each other. However, this is less than a quarter of the 1.5 GHz synthesized beam and considering that the 4σ contours overlap, we feel that it is highly unlikely that both sources are not α Boo.

3.2. *α Tau Radio Maps*

The final deconvolved radio maps of α Tau were of excellent quality with the rms noise reaching the predicted thermal noise in many cases. The target field at all frequencies was free from strong serendipitous radio sources and thus the final images were free of the sidelobe contamination that were present in the low frequency α Boo images. α Tau was the only source in the high frequency maps while the brightest source in the low frequency maps was located $106''$ north north-east of α Tau and had flux densities of 0.85, 1.35, and 1.7 mJy at 8.5, 5.0, and 3.5 GHz, respectively. Strong detections ($> 14\sigma$) of α Tau were made at all frequencies between 5.0 and 43.3 GHz. Due to the limited number of S-band receivers installed at the time, a full 2.5 hr track was dedicated to α Tau at 3.1 GHz in order to achieve the required sensitivity to give a possible detection. We report a tentative 3σ detection of α Tau at 3.1 GHz when we take its peak pixel value as its total flux density. As this is a weak detection we avoid using the *imfit* task to obtain a flux density estimate, as this may introduce further errors (Taylor et al. 1999).

4. DISCUSSION

4.1. *Results Versus Previous Observations*

Prior to and during the early operation of the 'old' VLA, a small number of single dish radio observations reported the detection of flares from single red giants (e.g. Boice et al. 1981). These transient radio events have never been re-observed however, even with more sensitive interferometers, suggesting that such detections were false (e.g. Beasley et al. 1992). The first definitive detection of thermal free-free emission from a single red giant at centimeter wavelengths was of α Boo at 6 cm (Drake & Linsky 1983, 1986). Since then there has been a modest number of sporadic centimeter and millimeter observations of this star. In Table 4 we list the majority of these observations and plot their flux densities as a function of frequency in Figure 1. In comparison to other single red giants, α Boo had been relatively well observed at radio wavelengths before this study, including detections in four VLA bands (i.e. Q, K, Ku, and C). No Ku band receivers were available during the commissioning phase of the VLA in early 2011 so we can compare three of our detections with previous ones.

Previous detections at 6 cm ranged from a 3σ upper limit of 0.18 mJy to a 3σ detection at 0.39 mJy. Our 6 cm value agrees to within $\sim$10% of the highest S/N (5σ) value of Drake & Linsky (1986). There is no significant difference between our 1.3 cm value and that of Dehaes et al. (2011). There is however a notable difference in flux density values at 0.7 cm where Dehaes et al. (2011) report values that are lower than ours by over 40%. Such a level of chromospheric variability seems rather high and would be unexpected from such supposedly inactive stars. Another possibility for the difference in values is that the longer cycle time used by Dehaes et al. (2011), which was over double our value, may cause larger phase errors and thus lower final flux density values. Future high frequency VLA observations of α Boo will clarify this discrepancy at 0.7 cm but past detections at longer wavelengths appear to be in good agreement with our data.

Prior to this study, α Tau had only been detected at two VLA bands (i.e. X and Ku) and had never been detected at wavelengths longer than 3 cm due to its weakly ionized wind. The lack of a Ku measurement means that we can only compare the previous 3 cm detection of Brown & Harper (1997) to ours. We find that there is no significant difference between the two. Interestingly however, Brown & Harper (1997) failed to detect α Tau at 6 cm but placed a 3σ upper limit of 0.07 mJy on its emission. In stark contrast to this, we were able to detect the star at 6 cm with a flux density over two times greater than this value. This hint of variability at long wavelengths can only again be confirmed with future high S/N observations.

Table 4
Compilation of Previous Radio Observations of α Boo and α Tau ($\nu \leq 250$ GHz)

	Frequency (GHz)	Date	Flux Density (mJy)	Source
α Boo (K2 III)	4.9	1983 Jan 21	0.39 ± 0.13	Drake & Linsky (1986)
	4.9	1983 May 20	0.26 ± 0.08	Drake & Linsky (1986)
	4.9	1983 Dec 26	$\leq 0.18(3\sigma)$	Drake & Linsky (1986)
	4.9	1984 Mar 17	0.24 ± 0.05	Drake & Linsky (1986)
	15.0	1984 Nov 6	0.68 ± 0.09	Drake & Linsky (1986)
	22.5	1999 Jan 06	1.7 ± 0.2	Dehaes et al. (2011)
	43.3	1999 Jan 06	3.3 ± 0.4	Dehaes et al. (2011)
	43.3	2004 Jan 25	3.34 ± 0.08	Dehaes et al. (2011)
	86.0	1985 Nov	21.4 ± 7.5	Altenhoff et al. (1986)
	108.4	1997 Nov - 2000 Jun	20.09 ± 0.69	Cohen et al. (2005)
	217.8	1997 Nov - 2000 Jun	83.5 ± 1.71	Cohen et al. (2005)
	250.0	1986 Dec - 1989 Mar	78 ± 8	Altenhoff et al. (1994)
α Tau (K5 III)	4.9	1983 Jan 21	$\leq 0.27(3\sigma)$	Drake & Linsky (1986)
	4.9	1984 Nov 6	$\leq 0.22(3\sigma)$	Drake & Linsky (1986)
	5.0	1997 Sep 27	$\leq 0.07(3\sigma)$	Brown & Harper (priv. comm.)
	8.5	1997 Sep 27	0.28 ± 0.03	Brown & Harper (priv. comm.)
	14.9	1997 Sep 27	0.95 ± 0.08	Brown & Harper (priv. comm.)
	15.0	1984 Nov 6	0.60 ± 0.1	Drake & Linsky (1986)
	108.4	1997 Nov - 2000 Dec	13.97 ± 1.46	Cohen et al. (2005)
	217.8	1999 Sep - 2000 Dec	25.78 ± 5.64	Cohen et al. (2005)
	250.0	1986 Dec - 1987 Jan	51 ± 6	Altenhoff et al. (1994)

4.2. *Existing Atmospheric Models*

One of the most important diagnostic features indicating mass outflows in late type stars are the blue shifted absorption components present in the Mg II h and k resonance lines. Figure 1 shows the predicted radio spectrum from the chromosphere and wind models of Drake (1985), which were based on the Mg II k 2796 Å emission line taken with the the International Ultraviolet Explorer. Both of Drake's models predict the wind to reach a terminal velocity of 40 km s^{-1} at ~ 2 $R_\star$ and have a broad temperature plateau with T $\approx$ 8,000 K between 1.2 and ~ 13 $R_\star$ with a cooler region further out. At high frequencies the models predict the slope of the spectral energy distribution to be blackbody-like (i.e. $\sim \nu^2$) as a result of the small density scale heights close to the star. At low frequencies however, the models predict the wind to have constant velocity, ionization and temperature and thus the slope approaches the well known $\sim \nu^{0.6}$ limit (Wright & Barlow 1975; Olnon 1975; Panagia & Felli 1975). The paucity and, in some cases low S/N, of previous observations made it difficult to discern the validity of this model prior to our multi-frequency study of α Boo. Our new data reveal significant deviations from the current existing semi-empirical model at both low and high frequencies (in this case below $\sim$ 8 GHz and above $\sim$ 25 GHz). At high frequencies our VLA data indicates a flux excess which is in agreement with previous mm-observations. The discrepancy at low frequencies may indicate that we are still sampling a region of the wind where it is still accelerating (i.e. it has not yet reached its terminal velocity) or may also be a manifestation of rapid wind cooling further out than that predicted in UV spectral analysis. We will discuss these possibilities in the following sections.

In Figure 2 we plot the expected thermal radio continuum spectrum produced by the semi-empirical 1-D chromospheric model of McMurry (1999) embedded in the wind model of Robinson et al. (1998). The McMurry model includes a transition region and reaches a maximum temperature of 10^5 K at 1.2 $R_\star$. Beyond this we assume an outflow with a constant temperature of 8,000 K reaching a terminal velocity of 30 km s^{-1} at 3 $R_\star$. The combination of these atmospheric models result in a predicted excess of radio emission at high frequencies (i.e. $>$ 30 GHz) but does a good job in reproducing the VLA fluxes below 30 GHz. The VLA, Institut de Radioastronomie Millimétrique (IRAM) 30 m-telescope and Berkeley Illinois Maryland Association (BIMA) continuum fluxes confirm that this model predicts a flux excess at even higher frequencies. One possible explanation for this is that the inner atmosphere contains extensive cooler gas than that predicted by the 1-D static chromospheric model of McMurry. This scenario agrees with the findings of Wiedemann et al. (1994) who conclude that cool regions exist close to the stellar surface with large filling factors (i.e. a thermally bifurcated CO-mosphere). For α Boo there is a hint that the transition frequency between wind and chromosphere occurs at about 8.5 GHz due to the change of slope but for α Tau, with its low mass loss rate giving rise to a low wind opacity, this is harder to distinguish. There is a small hint that this may occur at 6 cm and a higher S/N detection at 13 cm would confirm this.

We also include the predicted radio spectrum from the theoretical Alfvèn wave driven outflow model for α Tau (Krogulec 1989) in Figure 2 to demonstrate how radio observations can test the robustness of theoretical models. This model is based on a larger than now expected mass loss rate for the star (i.e 6.3×10^{-9} $M_\odot$ yr^{-1}) and predicts a fully ionized outflow. As the radio opacity is proportional to $n_e n_{ion}$ this model greatly over estimates the actual radio flux density at all VLA wavelengths. The same result is to be expected from the Alfvèn wave model of α Boo (Krogulec 1988).

4.3. *Radio Spectral Indices*

For a thermal source which has a constant electron density distribution, its radio emission has a well defined spectral index α ($F_\nu \propto \nu^\alpha$). For an optically thick ho-

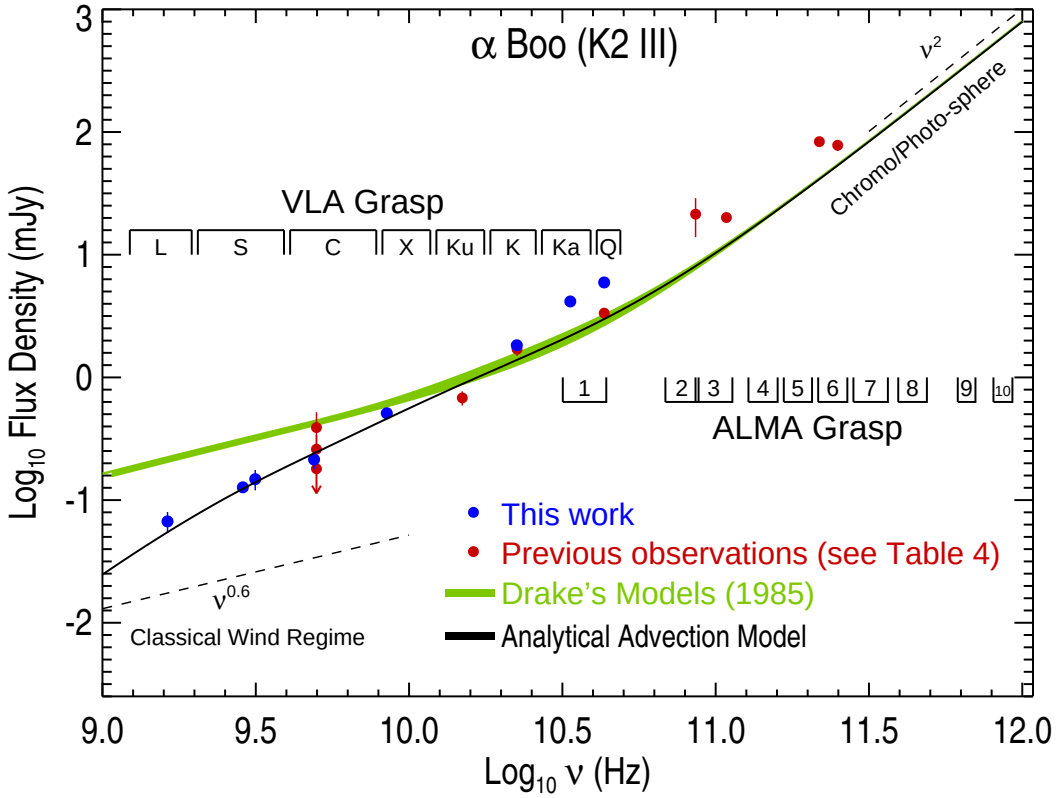

Figure 1. Spectral energy distribution of α Boo for frequencies less than 250 GHz. Our new multi-wavelength VLA observations which were mainly acquired over a few days in February 2011 are the blue circles and are in disagreement with the existing chromospheric and wind models of Drake (1985). The overlap between the two models are represented by the green shaded area. The red circles are previous observations which were acquired sporadically over the past $\sim$ 25 years with the 'old' VLA, IRAM and BIMA. The black line is the expected radio emission from the Drake model which undergoes rapid wind cooling at $\sim$ 2.3 $R_\star$ (see Section 4.3 and 4.4).

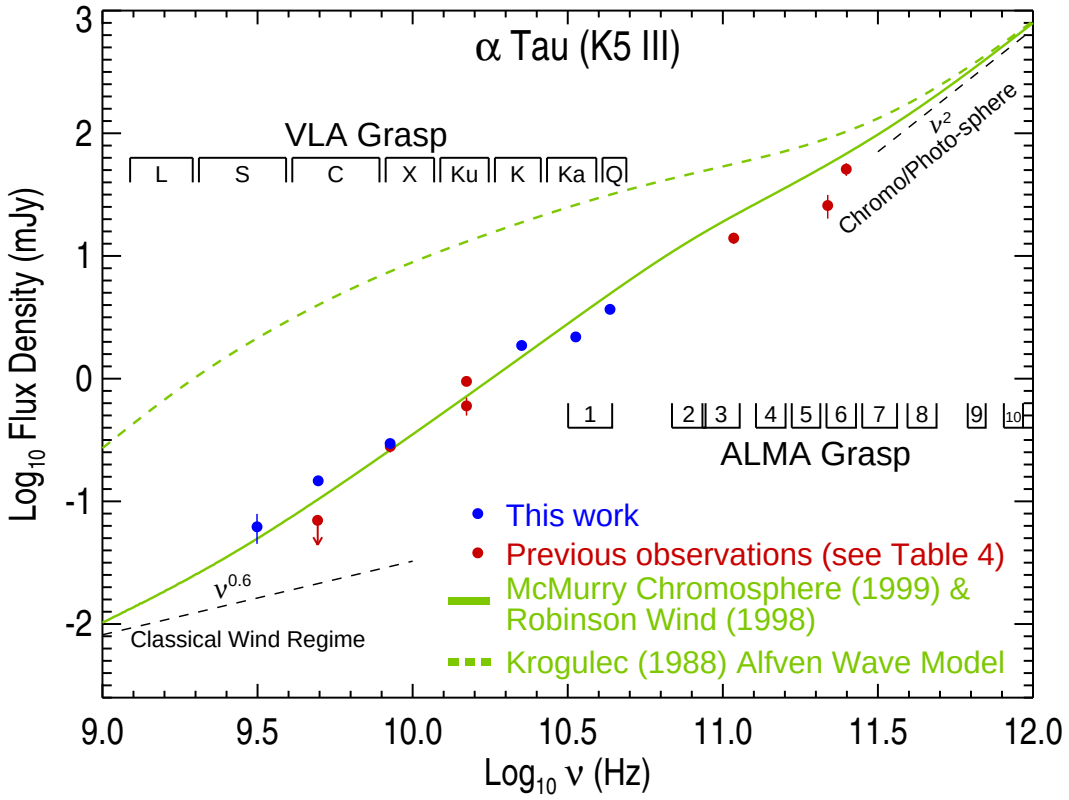

Figure 2. Spectral energy distribution of α Tau for frequencies less than 250 GHz. All our new α Tau multi-wavelength VLA observations (blue circles) were acquired in just two days in February 2011. The red circles are the previous observations which were acquired over many years. The green line is an existing hybrid chromosphere and wind model for the star.

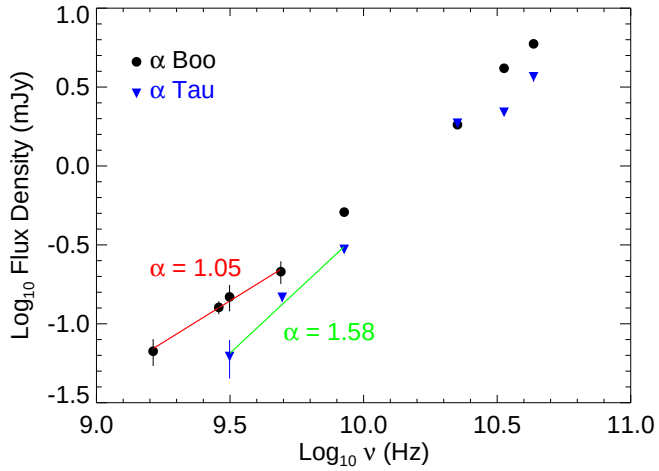

Figure 3. Radio spectra for α Boo and α Tau, together with the best fit straight lines to their long wavelength flux densities and the resulting spectral indices.

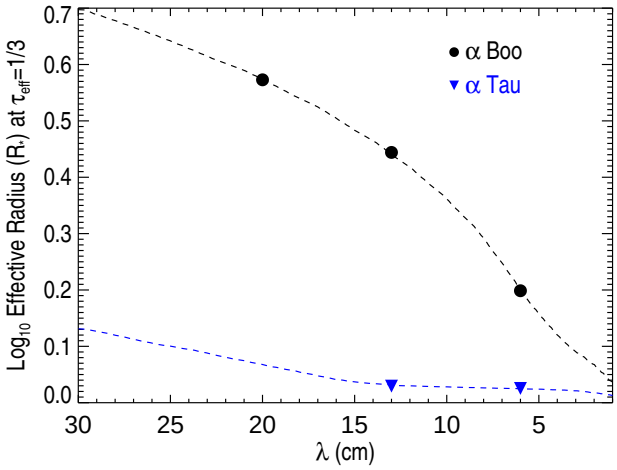

Figure 4. Predicted effective radius (dashed lines) as a function of wavelength for α Boo and α Tau. Points corresponding to our long wavelength VLA measurements are also shown. At the same radio wavelengths the less ionized mass outflow of α Tau results in a smaller effective radius than α Boo.

mogeneous plasma α follows the Rayleigh-Jeans tail of the Planck function (i.e. $\alpha = +2$), while for an optically thin homogeneous plasma $\alpha = -0.1$. However, the electron density in the mass outflow region of a star is not constant as a function of radius and usually varies by many orders of magnitude. It has been shown (Wright & Barlow 1975; Olnon 1975; Panagia & Felli 1975) that the expected radio spectrum from such a mass outflow region varies as $\nu^{0.6}$, where a spherically symmetric isothermal mass outflow with a uniform velocity is assumed. If we relax these assumptions and instead assume that the electron density and temperature profiles vary as a function of distance from the star r, and have the form $n_e \propto r^{-p}$ and $T_e \propto r^{-n}$ respectively, where $p > 1.5$ then

$$\alpha = \frac{4p - 6.2 - 0.6n}{2p - 1 - 1.35n} \qquad (1)$$

(e.g. Seaquist & Taylor 1987). In doing this, we are assuming that the ionization fraction is constant throughout the outflow. Thus, by assuming either a constant velocity (i.e. $p = 2$) or an isothermal outflow (i.e. $n = 0$), we can easily estimate the power-law decay of either the temperature or velocity profile, respectively.

The radio spectra for both stars are shown in Figure 3, together with the straight lines that were fitted to the long wavelength flux densities by minimizing the chi-square error statistic. For α Boo a straight line with $F_\nu \propto \nu^{1.05\pm x}$ fits the four longest wavelength data points well. This spectral index is larger than the 0.8 value obtained by Drake & Linsky (1986) whose value was based on a shorter wavelength (2 cm) value and a mean value of four low S/N measurements at 6 cm. α Tau was found to have a larger spectral index and a straight line with $S_\nu \propto \nu^{1.58\pm x}$ best fitted the three longest wavelength data points. This value is in agreement with Drake & Linsky (1986) who report a value ≥ 0.84 and is lower than the value of 2.18 that can be derived from the shorter wavelength data provided by Brown & Harper (priv. Comm.). These new spectral indices were then used in conjunction with Equation 1 to obtain the density and temperature coefficients listed in Table 5.

Table 5
Radio Spectral Indices and Resulting Density and Temperature Coefficients.

Star	Spectral index α	Density coefficient p	Temperature coefficient n
α Boo	1.05	2.71	1.65
α Tau	1.58	5.50	1.92

For an isothermal, constant velocity wind, Equation 1 implies $\alpha = 0.6$. The fact that our derived values are substantially larger implies at least one of the assumptions regarding the wind's properties are false. A common explanation in the literature for spectral indices larger than 0.6 is that the wind is still accelerating in the region where the radio emission is emanating from and thermal gradients are ignored. If this is also the case here, then the density obeys a power-law falloff with coefficients listed in column 3 of Table 5. This assumption is reasonable at short wavelengths where the majority of the radio emission is expected to emanate within the wind's acceleration zone, but at long VLA wavelengths (i.e. between 6 and 20 cm) this assumption might be false and we may indeed be sampling the wind very close to or at its terminal velocity.

To investigate this matter further, we estimate the effective radius of the radio emitting region per wavelength based on the Drake model for α Boo and the hybrid McMurry and Robinson model for α Tau. We follow the approach used by Cassinelli & Hartmann (1977) and assume that the radio emission at any wavelength emanates from a surface at effective optical depth $\tau_{\rm eff} = 1/3$. Since the radio free-free opacity increases at longer wavelengths (i.e. $\kappa \propto \lambda^{2.1}$) the optical depth along a line of sight into the stellar outflow also increases at longer wavelengths. This implies that the effective radius (i.e. the radius where $\tau = \tau_{\rm eff}$) will increase with longer wavelengths and will be greater for outflows with higher ionization densities as $\tau \propto \int \lambda^{2.1} n_{\rm ion} n_{\rm e} dr$.

The higher degree of ionization in the mass outflow

of α Boo in comparison to α Tau makes a substantial difference to the size of the stars effective radius as can be seen in Figure 4. At 6, 13, and 20 cm the effective radius of α Boo is predicted to be 1.6, 2.8, and 3.7 $R_\star$ while is only ~ 1.1 $R_\star$ at 6 and 13 cm for α Tau. Robinson et al. (1998) predict that α Tau's wind does not reach its terminal velocity until 3 $R_\star$? while the transition region in the model of McMurry (1999) begins at 1.2 $R_\star$, so it appears unlikely that even our longest wavelength VLA measurements of α Tau sample its outer wind. For α Boo however, Drake (1985) predicts that the wind has reached its terminal velocity by ~ 2 $R_\star$ so based on this model, our longest VLA measurements probable sample its wind at (or very close to) its terminal velocity. Our spectral index would then indicate that the wind is cooling as it expands with a constant velocity and has a temperature coefficient of 1.65.

4.4. *Analytical Advection Model for α Boo's Wind*

A failure of the existing atmospheric model for α Boo is that is overestimates the radio fluxes at long VLA wavelengths as clearly shown in Figure 1. If these wavelengths are indeed sampling the wind at its terminal velocity then a reason for this overestimation may be that the wind is cooling closer in than that predicted by the model. The main mechanism for this cooling would be wind expansion (O'Gorman & Harper 2011) and would cause lower electron densities than those predicted by the existing model due to larger recombination rates. To investigate this possibility further we adjusted the existing model to include a temperature power-law falloff of the form

$$T_e(r) = T_e(r_1)\left(\frac{r_1}{r}\right)^{1.65}, \qquad (2)$$

where r_1 is just an arbitrary distance from the star and the temperature coefficient is that obtained from our new VLA data (see Table 5). To calculate the new $n_{\rm e}$ and $n_{\rm ion}$ densities in the wind regime where this temperature falloff occurs, we used the analytical expression of Glassgold & Huggins (1986) to calculate the hydrogen ionization fraction, $x_{\rm H}$. In doing so we need to make a number of assumptions about the wind properties from r_1 onwards.

- We assume a conserved mass outflow i.e. $n_{\rm H}(r) = C/r^2$ where $n_{\rm H}$ is the total hydrogen number density and C is a constant proportional to the ratio of the mass loss rate divided by the terminal velocity. For α Boo, $C = 1.5 \times 10^{32}$ cm^{-1}.
- We assume that all ionization processes cease.
- We consider only radiative recombination of H and include the temperature variation of the recombination coefficient α^b which excludes captures to the n=1 level (Spitzer 1978).
- We assume a constant heavy ion fraction, $x_{\rm hi} = 10^{-4}$.

Using these assumptions it can be shown that

$$x_{\rm H}(r) = \frac{x_{\rm H}(r_1)x_{\rm hi}e^{-I}}{x_{\rm hi} + x_{\rm H}(r_1)(1-e^{-I})} \qquad (3)$$

Table 6
Ionized mass loss rates for α Boo and α Tau.

Star	Wavelength (cm)	$\dot{\rm M}_{\rm ion}$ (M$_\odot$ yr^{-1})
α Boo	6.0	5.9×10^{-11}
	9.5	5.5×10^{-11}
	10.0	5.1×10^{-11}
	20.0	4.3×10^{-11}
α Tau	6.0	$\leq 8.2 \times 10^{-11}$
	9.5	$\leq 5.3 \times 10^{-11}$

where

$$I = 2.38 \times 10^{-3}\left[\left(\frac{r_1}{r}\right)^{-0.19} - 1\right], \text{ and } \ {\rm r} \geq {\rm r}_1. \qquad (4)$$

If we alter the existing Drake model so that it now has a narrower temperature plateau of $T_e = 10,000$ K between 1.2 and 2.3 $R_\star$, a temperature profile given by Equation 2 and a density profile governed by Equation 3 beyond 2.3 $R_\star$, then we get a good agreement with our new long wavelength VLA data as shown in Figure 1.

Encouraging as it is that such a simple analytical model can reproduce values close to the observed radio fluxes at long wavelengths, it must be stressed that this *hybrid* model is just a first order approximation. It still does not reproduce the radio fluxes at wavelengths shorter than ~ 3 cm and therefore a new atmospheric model is still required that can reproduce all the observed fluxes. To do so, the non-trivial task of simultaneously solving the non-local radiative transfer equation and atomic rate equations which include advection will be required.

4.5. *Ionized Mass Loss Rates*

For a partially ionized outflow, such as that expected from α Boo and α Tau, the ionized mass loss rate can be estimated from the radio emission assuming a constant velocity, constant temperature, and constant ionization fraction and can be written as

$$\dot{M}_{\rm ion} \simeq 5.58 \times 10^{-14}\left(\frac{v_\infty}{\rm km\ s^{-1}}\right)\left(\frac{D}{\rm pc}\right)\left(\frac{F_\nu}{\rm mJy}\right)^{0.75} \times \left(\frac{\lambda}{\rm cm}\right)^{0.45}\left(\frac{T_{\rm e}}{10^4{\rm K}}\right)^{0.1} \dot{M}_\odot\ {\rm yr}^{-1} \qquad (5)$$

where D is the distance and v_∞ is the wind terminal velocity defined earlier in Table 1. Using this expression, the ionized mass loss rates were derived for each of the long wavelength measurements for both stars and are listed in Table 5. These values are based on the assumption of a $T_{\rm e} = 10^4$ K wind for both stars.

We have have discussed in the previous sections that for α Boo, these long wavelengths sample the outer atmosphere of the star where the wind is close to or has reached its terminal velocity and is beginning to cool due to gas expansion. In this case, these $\dot{M}_{\rm ion}$ values would be lower than those given in 6. However, as $\dot{M}_{\rm ion}$ is only weakly dependent on $T_{\rm e}$ this makes only a small difference and amounts to about a 7% increase in the ionized mass loss if the temperature is actually lower by 50%. If the ionization balance is frozen-in in the regions of the outflow where these long wavelengths sample then the derived $\dot{M}_{\rm ion}$ should be the same for these wavelengths.

The decrease in $\dot{M}_{\rm ion}$ with longer wavelengths as seen in Table 6 is probably therefore due to a combination of lower temperatures and lower ionization fractions further out in the atmosphere. The ionized mass loss rates for α Tau given in Table 6 are derived assuming the radio emission emanates from the outer atmosphere where the wind has reached its terminal velocity. As discussed in Section 4.3 the longest wavelengths are still sampling the acceleration zone and thus these ionized mass loss rates are just upper limits.

5. CONCLUSIONS

The data presented in this paper were obtained with the Karl G. Jansky Very Large Array (VLA) which is an instrument of the National Radio Astronomy Observatory (NRAO). The NRAO is a facility of the National Science Foundation operated under cooperative agreement by Associated Universities, Inc. We wish to thank the NRAO helpdesk for their detailed responses to our CASA related queries.

Facilities: VLA.

REFERENCES

Altenhoff, W. J., Huchtmeier, W. K., Schmidt, J., Schraml, J. B., & Stumpff, P. 1986, A&A, 164, 227
Altenhoff, W. J., Thum, C., & Wendker, H. J. 1994, A&A, 281, 161
Ayres, T. R., Linsky, J. L., Vaiana, G. S., Golub, L., & Rosner, R. 1981, ApJ, 250, 293
Baade, R., Kirsch, T., Reimers, D., Toussaint, F., Bennett, P. D., Brown, A., & Harper, G. M. 1996, ApJ, 466, 979
Beasley, A. J., Stewart, R. T., & Carter, B. D. 1992, MNRAS, 254, 1
Boice, D. C., Kuhn, J. R., Robinson, R. D., & Worden, S. P. 1981, ApJ, 245, L71
Cassinelli, J. P., & Hartmann, L. 1977, ApJ, 212, 488
Chapman, R. D. 1981, ApJ, 248, 1043
Cohen, M., Carbon, D. F., Welch, W. J., Lim, T., Schulz, B., McMurry, A. D., Forster, J. R., & Goorvitch, D. 2005, AJ, 129, 2836
Crowley, C., Espey, B. R., Harper, G. M., & Roche, J. 2009, in American Institute of Physics Conference Series, Vol. 1094, 15th Cambridge Workshop on Cool Stars, Stellar Systems, and the Sun, ed. E. Stempels, 267–274
Crowley, C., Espey, B. R., & McCandliss, S. R. 2008, ApJ, 675, 711
Dehaes, S., et al. 2011, A&A, 533, A107
di Benedetto, G. P. 1993, A&A, 270, 315
Drake, S. A. 1985, in Progress in stellar spectral line formation theory; Proceedings of the Advanced Research Workshop, Trieste, Italy, September 4-7, 1984 (A86-37976 17-90). Dordrecht, D. Reidel Publishing Co., 1985, p. 351-357., ed. J. E. Beckman & L. Crivellari, 351–357
Drake, S. A., & Linsky, J. L. 1983, ApJ, 274, L77
—. 1986, AJ, 91, 602
Eaton, J. A. 2008, AJ, 136, 1964
Falceta-Gonçalves, D., Vidotto, A. A., & Jatenco-Pereira, V. 2006, MNRAS, 368, 1145
Glassgold, A. E., & Huggins, P. J. 1986, ApJ, 306, 605
Harper, G. M. 2010, ApJ, 720, 1767
Harper, G. M., Brown, A., Bennett, P. D., Baade, R., Walder, R., & Hummel, C. A. 2005, AJ, 129, 1018
Hartmann, L., & MacGregor, K. B. 1980, ApJ, 242, 260
Holzer, T. E., & MacGregor, K. B. 1985, in Astrophysics and Space Science Library, Vol. 117, Mass Loss from Red Giants, ed. M. Morris & B. Zuckerman, 229–255
Judge, P. G., & Carpenter, K. G. 1998, ApJ, 494, 828
Krogulec, M. 1988, , 38, 107
—. 1989, , 39, 51
Linsky, J. L., & Haisch, B. M. 1979, ApJ, 229, L27
McMullin, J. P., Waters, B., Schiebel, D., Young, W., & Golap, K. 2007, in Astronomical Society of the Pacific Conference Series, Vol. 376, Astronomical Data Analysis Software and Systems XVI, ed. R. A. Shaw, F. Hill, & D. J. Bell, 127
McMurry, A. D. 1999, MNRAS, 302, 37
O'Gorman, E., & Harper, G. M. 2011, in Astronomical Society of the Pacific Conference Series, Vol. 448, 16th Cambridge Workshop on Cool Stars, Stellar Systems, and the Sun, ed. C. Johns-Krull, M. K. Browning, & A. A. West, 691
Olnon, F. M. 1975, A&A, 39, 217
Panagia, N., & Felli, M. 1975, A&A, 39, 1
Robinson, R. D., Carpenter, K. G., & Brown, A. 1998, ApJ, 503, 396
Seaquist, E. R., & Taylor, A. R. 1987, ApJ, 312, 813
Spitzer, L. 1978, Physical processes in the interstellar medium
Sutmann, G., & Cuntz, M. 1995, ApJ, 442, L61
Suzuki, T. K. 2007, ApJ, 659, 1592
Taylor, G. B., Carilli, C. L., & Perley, R. A., eds. 1999, Astronomical Society of the Pacific Conference Series, Vol. 180, Synthesis Imaging in Radio Astronomy II
van Leeuwen, F. 2007, A&A, 474, 653
Wiedemann, G., Ayres, T. R., Jennings, D. E., & Saar, S. H. 1994, ApJ, 423, 806
Wright, A. E., & Barlow, M. J. 1975, MNRAS, 170, 41